Activation Energies for Oxygen Reduction on Platinum Alloys: Theory and Experiment

Alfred B. Anderson* and Jérôme Roques

Chemistry Department, Case Western Reserve University, 10900 Euclid Avenue, Cleveland, Ohio 44106-7078

Sanjeev Mukerjee‡ and Vivek S. Murthi

Chemistry Department, 102 Hurtig Hall, Northeastern University, Boston, Massachusetts 02115-5000

Nenad M. Markovic§ and Vojislav Stamenkovic

Materials Science Division, Lawrence Berkeley National Laboratory, University of California, Berkeley, California 94720

Received: June 11, 2004; In Final Form: October 20, 2004

A combined theoretical and experimental analysis of the electrode potential dependencies of activation energies is presented for the first step in oxygen reduction over platinum and platinum alloy catalysts in both polycrystalline and carbon supported form. Tafel data for several of the catalysts are used to predict potential-dependent activation energies for oxygen reduction over the 0.6−0.9 V range in strong and weak acid. Comparisons with the theoretical curve show good agreement above 0.8 V, suggesting a fairly constant preexponential factor. Arrhenius determinations of activation energies over the 0.7−0.9 V range yield little trend for weak acid, possibly because of the larger uncertainties in the Arrhenius fits, but the strong acid results have smaller uncertainties and for them the measured activation energies trend up with potential.

I. Introduction

Recent theoretical studies by Anderson and co-workers of oxygen reduction over 1-fold[1] and 2-fold[2] sites on platinum surfaces have lent support to the proposition that the first reduction step

$$O_2(ads) + H^+(aq) + e^-(U) \rightarrow OOH(ads) \qquad (1)$$

where U is the electrode potential, has a higher activation energy than subsequent steps. This prediction held in the overpotential region typical of oxygen cathodes in fuel cell applications, which is ∼0.7 to 0.9 V on the hydrogen scale (used throughout this paper). According to ref 1, in the case of 1-fold sites, which have just a single coordination site to a single platinum atom available, the second reduction forms weakly adsorbed H_2O_2, which leaves the surface. According to ref 2, when a dual Pt site is present OOH(ads) adsorbs bridging the Pt atoms sites and dissociates with a small activation energy. The theoretical procedure used in these studies was a newly developed one that uses a local reaction center model and yields activation energies as functions of electrode potential for electron-transfer reactions.[1−5] The calculated activation energy at 1.23 V was 58 kJ/mol (Table 1),[2] which was close to the extrapolated experimental apparent activation energy value of 42 kJ/mol on Pt(111) in 0.05 M H_2SO_4.[6] As will be discussed below, a recent more extensive transition state search has found a lower value for the activation energy of 50 kJ mol^{-1} at the reversible potential. The low activation energies found for PtOH and Pt_2O reduction confirm the earlier theoretical work.[1]

TABLE 1: Calculated Activation Energies as a Function of the Electrode Potential for the First Step of O_2 Reduction ($Pt_2O_2 + H^+_{(aq)} + E^-(U) \rightarrow Pt_2OOH$)[2,43]

	activation energy	
potential (V)	kJ/mol	eV
0.47	0.00	0.00
0.60	5.25	0.05
0.66	8.42	0.09
0.71	11.03	0.11
0.76	13.89	0.14
0.81	17.08	0.18
0.86	20.49	0.21
1.01	31.70	0.33
1.16	43.75	0.45
1.30	56.44	0.59

Poisoning, i.e., site blocking, of the platinum surface by OH-(ads) formed from water oxidation by the reaction

$$H_2O(ads) \rightarrow OH(ads) + H^+(aq) + e^-(U) \qquad (2)$$

commences at ∼0.6 to 0.7 V.[7,8] There is voltammometric evidence for OH(ads) formation over each of the three low-index Pt(111), Pt(100), and Pt(110) surfaces.[9]

Several investigations have been carried out to determine the role of alloying on the oxygen reduction reaction (ORR). Alloying is believed to retard the formation of the OH(ads) electrode surface poison. Mukerjee et al. investigated five carbon-supported binary Pt alloy nanocluster electrocatalysts (PtCr, PtMn, PtFe, PtCo, and PtNi) and found enhanced electrocatalytic activity for ORR on these five binary Pt alloys compared to Pt/C electrocatalysts.[10,11] The electrocatalytic activities decreased in the order PtCr/C > PtFe/C > PtMn/C >

* Address correspondence to this author. E-mail: aba@po.cwru.edu. Phone: 216 368 5044. Fax: 216 368 3006.

‡ E-mail: smukerjee@lynx.neu.edu. Phone: 617 373 2382. Fax: 717 373 8949.

§ E-mail nmmarkovic@lbl.gov. Phone: 510 495 2956. Fax: 510 486 4793.

10.1021/jp047468z CCC: $30.25
Published on Web 01/04/2005

TABLE 2: Experimental Activation Energies for the Oxygen Reduction Reaction on Carbon-Supported Alloy Catalysts from the Work of Paulus et al.[12] in 0.1 M $HClO_4$

		activation energy	
catalyst	potential (V)	kJ/mol	eV
Pt/C	0.93	21	0.22
Pt_3Ni/C	0.93	24	0.25
PtCo/C	0.93	24	0.25
Pt_3Co/C	0.93	25	0.26
Pt/C	0.88	20	0.21
Pt_3Ni/C	0.88	22	0.23
PtCo/C	0.88	28	0.29
Pt_3Co/C	0.88	28	0.29
Pt/C	0.83	23	0.24
Pt_3Ni/C	0.83	26	0.27
PtCo/C	0.83	24	0.25
Pt_3Co/C	0.83	26	0.27

TABLE 3: Experimental Activation Energies for the Oxygen Reduction Reaction on Well-Defined Pt_3Ni and Pt_3Co Alloy Surfaces with a Pt Skin (annealed surfaces) and without a Pt Skin (sputtered surfaces), from the Work of Stamenkovic et al.[13] in 0.1 M $HClO_4$

		activation energy	
catalyst	potential (V)	kJ/mol	eV
Pt-polycrystalline	0.93	21	0.22
Pt_3Ni-sputtered	0.93	23	0.24
Pt_3Co-sputtered	0.93	22	0.23
Pt_3Co-annealed	0.93	25	0.26

PtCo/C > PtNi/C > Pt/C. On the basis of extended X-ray fine structure analysis, Mukerjee and co-workers proposed that the catalyst particles were coated with a platinum skin in which the electronic properties of the surface Pt atoms are modified by the subsurface alloying atoms to reduce the formation of OH(ads).

Paulus et al. characterized carbon-supported Pt−Ni and Pt−Co catalysts microscopically by high-resolution transmission electron spectroscopy and electrochemically by temperature-dependent oxygen reduction Tafel plot measurements.[12] They found Arrhenius apparent activation energies for 0.1 M perchloric acid electrolyte at 0.93 V of 21 kJ/mol for Pt/C, 24 kJ/mol for Pt_3Ni/C, 25 kJ/mol for Pt_3Co/C, and 24 kJ/mol for PtCo/C. Activities for oxygen reduction paralleled the Mukerjee finding with PtCo/C > Pt_3Co/C > Pt_3Ni/C > Pt/C. Paulus et al. noted that these activation energies were similar to one another and proposed that the preexponential factor in the Arrhenius rate expression determined the variations in observed rates and that this effect could be associated with surface site blocking by OH(ads). Activation energies were also determined for the potentials 0.88 and 0.83 V (Table 2) on the SHE scale with a maximum deviation from the above values of 0.4 kJ mol^{-1}; there was no uniform trend in the values as functions of electrode potential. The five data points in each of the Arrhenius plots showed scattering and the reported activation energies had uncertainties of ± 2.5 kJ mol^{-1}.

More recently, catalytic activities of bulk Pt_3Ni and Pt_3Co alloy surfaces that were characterized in ultrahigh vacuum were studied in perchloric and sulfuric acid by Stamenkovic et al.[13] The activity of oxygen reduction in $HClO_4$ at 293 K again decreased in the order Pt_3Co > Pt_3Ni > Pt and the catalytic activity of Pt_3Co was a factor of 2 higher than that of pure Pt. Apparent activation energies in 0.1 M perchloric acid at 0.93 V were found from Arrhenius plots to be 21 kJ/mol for polycrystalline Pt, 23 kJ/mol for sputtered Pt_3Ni, 22 kJ/mol for sputtered Pt_3Co, and 25 kJ/mol for annealed Pt_3Co (Table 3). These values are close to those found at this potential in the work of Paulus et al. in ref 12. In sulfuric acid solution the order of activity changed to Pt_3Ni > Pt_3Co > Pt, indicating to Stamenkovic et al.[13] the possibility that bisulfate anion adsorption, along with OH(ads), was affecting the rate.

Recently Mukerjee and co-workers[14] have undertaken a study of oxygen reduction over Pt clusters and Pt-skin on Pt_3Fe and Pt_3Co clusters on carbon supports in trifluoromethane sulfonic acid, CF_3SO_3H (TFMSA). Results for 1 M TFMSA are presented in this paper. This gives an additional set of activation energies for carbon-supported catalysts in strong acid to compare with the carbon-supported catalysts in weak acid (Paulus et al.[12]) and bulk catalysts in weak acid (Stamenkovic et al.[13]).

The purpose of this paper is to compare predicted activation energies from ref 2 with experimentally determined values. The experimentally determined values for carbon-supported catalysts in ref 12 showed no trend with electrode potential and the values for polycrystalline electrodes in ref 13 were determined for only a single potential. However, the theoretical values of ref 2 clearly trended up in value as the electrode potential increased. Therefore, we take a two-pronged approach: Experimentally, new measurements have been made to determine with high precision the activation energies at 0.7, 0.75, 0.8, and 0.85 V for Pt, PtCo, and PtFe catalysts supported on carbon in strong acid. Theoretically, Tafel plots from these measurements and from those in ref 13 will be used to calculate, assuming a constant preexponential factor, the potential-dependent activation energies for comparison with predictions in ref 2.

II. Theoretical Approach

The activation energies, E_a, as a function of potential, U, $E_a(U)$, were determined as in ref 2, using spin unrestricted hybrid gradient corrected Becke, Lee, Yang, and Parr B3LYP density functional theory from Gaussian 94 with the 6-31G** basis set for light atoms.[15] An effective core potential and LANL2DZ basis set were used for the platinum atoms. As in past work, zero-point energies were neglected because the number of O−H bonds is conserved so that the net change for each reaction is small. The local reaction center model used in the study had the reduction precursor and transition state structures in the following equation

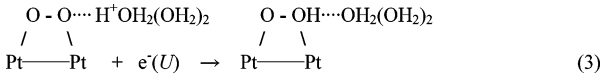

(3)

The transition states were found for each electrode potential U studied by finding the lowest energy structure for which the electron affinity, EA, of the local reaction system was given by the equation

$$\mathrm{EA} = eU + 4.6\ \mathrm{eV} \tag{4}$$

where 4.6 eV is the average thermodynamic work function of the standard hydrogen scale.[16] The calculations were performed with a structure constraint such that Pt_2OOH^+ and Pt_2OOH were in a plane, so that the twisting around the O−O axis that is characteristic of peroxide was not permitted. This is in recognition of the idea that the approach of the hydronium ion to O_2 adsorbed on the 2-fold Pt site will probably be sterically constrained at potentials >0.6 V by OH(ads). Two angles and five bond distances were varied in the calculations by pattern search and extrapolation. This procedure has been automated with a constrained variation program that employs Lagrange's method of undetermined multipliers.[17] The results in ref 2 have

been confirmed by using this program.[18] For this reduction reaction the reaction center EA must increase when the electrode potential is increased, and as shown in ref 2, this is accomplished by decreasing the $O\cdots H^+$ distance so as to stabilize the empty π^* orbital and increasing the H^+-OH_2 distance so as to increase the H^+ electron affinity, which in the limit of an isolated proton is 13.6 eV. The larger these distortions are, the greater is the activation energy.

To convert Tafel plots of electrode potential vs ln(i), where i is the current density, to activation energies we have made use of an equation similar to the Butler−Volmer equation. Instead of assuming that the activation energies for the forward and reverse reactions change linearly with electrode potential in the form $\beta\eta$ and $(1-\beta)\eta$, where β is independent of potential and η is the overpotential, we use calculated potential-dependent activation energies in the equation:

$$i(U) = |i_{ox}(U) - i_{red}(U)| = A|\exp(-E_a^{ox}(U)/RT) - \exp(-E_a^{red}(U)/RT)| \quad (5)$$

In the high reduction overpotential region considered in this work, the oxidation current will be small and will make little contribution to the net current density in eq 5. Taking the log of this equation yields an equation for predicting Tafel plots:

$$\log[i(U)] = \log(A) - E_a^{red}(U)/(2.3026RT) \quad (6)$$

When theoretical $E_a^{red}(U)$ are used in this equation to predict a Tafel plot, the preexponential factor A is determined by inputting one experimentally determined activation energy at some potential. Given an experimentally measured Tafel plot, $E_a^{red}(U)$ can be predicted at another potential through the use of eq 6.

III. Experimental Appoach

Full experimental details concerning catalyst preparation, characterization, and activation energy determinations for the carbon-supported and bulk catalysts in 0.1 M $HClO_4$ are in refs 12 and 13, respectively. Experimental details for the new results for 1 M CF_3SO_3H (TFMSA) reported here are presented next.

Two different carbon-supported binary Pt alloys, PtFe/C and PtCo/C, with a nominal composition of 3:1 (Pt:M) atomic ratio were investigated with Pt/C used as a control. All electrocatalysts were prepared in-house and had a metal loading of 20% on carbon support (Vulcan XC-72, Cabot, USA). The well-known colloidal "sol" and carbothermic reduction methods were used for catalyst preparation.[19−23] In these methods, an oxide of the second alloying element is incorporated on the supported Pt/C electrocatalyst. When this is subjected to carbothermic reduction under inert conditions at 900 °C, the crystallites undergo reduction and alloying on the carbon support, thus providing for supported alloy nanoparticles.

All electrochemical measurements were made with an Autolab (Ecochemie Inc., model PGSTAT 30) for both the rotating ring-disk electrode (Pine Instruments) experiments and in situ X-ray absorption spectroscopy (XAS). All potentials were measured with respect to a sealed hydrogen reference electrode (RHE).[24,25] To avoid potential artifacts, the electrolyte in the reference electrode had the same concentration as used in the experiment.

Trifluoromethane sulfonic acid (TFMSA) used as the electrolyte in this work was obtained from 3M Inc., and triply distilled under vacuum below 60 °C. The preparation of the electrode for RDE experiments involved a thin electrocatalyst layer on a glassy carbon electrode. Details of the distillation step and the thin electrocatalyst layer preparation for oxygen reduction kinetic measurements are given elsewhere.[14] Briefly, suspensions of 1 mg of catalyst in alcohol were obtained by ultrasonication for 30 min. A small amount of 5 wt % Nafion was added prior to this suspension to act as a binder. A 20-μL aliquot of the suspension was then loaded onto the glassy carbon (0.283 cm^2, Pine Instruments) to give a constant metal loading of 14 $\mu g/cm^2$ (geometric) and the electrode was allowed to dry at room temperature before introducing it into the electrolyte solution. This amount of catalyst to Nafion loading was very small compared to normal fuel cell electrodes (wt ratio of Pt to Nafion 50:1, mg/cm^2) and relative to previous rotating disk electrode experiments.[26,27]

After preparation, the electrodes were immersed in oxygen-free electrolyte solutions and cycled several times between 0 and 1.2 V (50 mV/s) at room temperature followed by further cycling at 10 mV/s prior to recording the cyclic voltammograms. For oxygen reduction studies at different temperatures, the electrode was immersed in oxygen-saturated electrolyte (Med-Tech Gases Inc.) at the respective temperature and scanned between 1.2 and 0.3 V at 25 mV/s for 10 cycles at each rotation rate (400, 625, 900, 1225, 1600, and 2500 rpm). The last 3 scans at each rotation rate were used for data analysis. Kinetic measurements of the ORR in terms of the Tafel parameters and kinetic currents were made at various temperatures (30, 40, 50, and 60 °C), similar to a wealth of prior published approaches for the analysis of the RDE data.[12,28,29]

Physicochemical Characteristics. The morphologies of the nanoparticles were investigated by using a combination of X-ray diffraction and in situ X-ray absorption spectroscopy (XAS), both conducted at the National Synchrotron Light Source (NSLS) in Brookhaven National Laboratory (Upton, NY). X-ray diffraction was conducted with use of the high-resolution X-18A beam line at the National Synchrotron Light Source (NSLS). Line broadening analysis of the primary XRD peak ⟨111⟩ was conducted by using the Scherrer treatment of the data. The data were first fitted to an indexing program, which allowed accurate measurement of the line widths at half-maximum. These widths were then used to obtain the particle size.

XANES (X-ray absorption near edge structure) data from in situ XAS were measured to verify the nominal atomic ratios as well as the nature of alloying, especially in the cases where the difference in the line shifts of the XRD patterns between Pt and Pt alloy electrocatalysts was very small. The methodology for analysis of the XANES spectrum followed those of Wong et al.[30]

A special in situ spectroelectrochemical cell, described in detail elsewhere,[31] was used, which allowed XAS measurements in transmission mode with the working electrode in a fully flooded state. XAS measurements were conducted at beam line X-11 A at the National Synchrotron Light Source (NSLS) in Brookhaven National Laboratory. Data were collected at both the Pt L (L_3 and L_2) and the alloying element K edges in the transmission mode, using incident, transmission, and reference ion chambers. A Pt foil at the reference detector provided accurate calibration and alignment of the edge positions. Details of the beam line optics and monochromator are given elsewhere.[32] The electrolyte of choice for in situ XAS measurements was 1 M $HClO_4$. Since the purpose of the XANES experiment was primarily to determine the atomic ratio of Pt and the alloying element as well as the d-band vacancy of Pt/atom, the in situ spectra was taken at 0.54 V vs RHE, being in the double layer region and close to the potential of zero charge. XAS data

TABLE 4: Structural Characteristics of the Pt and Pt Alloy Electrocatalyst with Powder XRD Data at 1.54 Å

electrocatalyst	lattice parameter	Pt−Pt bond distance (Å)	av particle size (Å)
Pt/C	3.927	2.777	25
PtCo/C	3.854	2.725	36
PtFe/C	3.866	2.733	39

TABLE 5: Results of XANES (at Pt L and K edge of allying metal) and EXAFS Analysis (at the Pt L_3 Edge) for Supported Pt and Pt Alloy Electrocatalysts[a]

electro-catalyst	atomic ratio (a/o) XANES	electrode potential (0.54 V vs RHE)		electrode potential (0.84 V vs RHE)	
		Pt−Pt (Å)	Pt−Pt (N)	Pt−Pt (Å)	Pt−Pt (N)
Pt/C		2.77	8.7	2.77	6.8
PtCo/C	72/28	2.68	6.9	2.68	7.6
PtFe/C	69/31	2.70	6.7	2.71	6.5

[a] All data were measured in situ at 0.54 and 0.84 V vs RHE in 1 M $HClO_4$. The windows for the Fourier transform parameters used for EXAFS analysis of Pt L_3 edge at 0.54 V are given as follows: Pt/C: $k^n = 3$; Δk (Å^{-1}) = 3.49−14.23; Δr (Å) = 1.4−3.05. PtCo/C: $k^n = 3$; Δk (Å^{-1}) = 3.22−14.61; Δr (Å) = 1.5−3.5. PtFe/C: $k^n = 3$; Δk (Å^{-1}) = 3.45−17.14; Δr (Å) = 1.5−3.4.

were also collected as a function of potential in the range of 0.0 to 1.2 V vs RHE for all the binary alloys in 1 M $HClO_4$. EXAFS analysis on the Pt L_3, Fe, and Co K edges followed methodologies developed by Koningsberger et al.,[33,34] the details of which are given elsewhere.[10,32,35,36] The effect of electrolyte environment on the electrocatalyst nanoclusters is not considered here and is the subject of a separate investigation. The use of $HClO_4$ in our in situ XAS experiments was based on its negligible anion adsorption[37,38] with 1 M concentration, a situation akin to the case with trifluoromethane sulfonic acid.[39−42]

Arrhenius Apparent Activation Energy Determination. All experimental apparent activation energies, E_a, for the oxygen reduction reaction over the various electrocatalysts were evaluated at fixed electrode potentials, U, using the Arrhenius equation:

$$\left(\frac{\partial \log(i_k)}{\partial(1/T)}\right)_U = \frac{E_a}{2.3R} \qquad (7)$$

where i_k is the kinetic current density, T is temperature, and R is the molar gas constant. Activation energies for carbon-supported catalysts in 0.1 M $HClO_4$ are in Table 2 (Paulus et al.[12]), and for polycrystalline electrodes, results are in Table 3 (Stamenkovic et al.[13]). Activation energies determined for 1 M CF_3SO_3H are shown in Table 6. The data in these three tables show activation energies in the range 0.2−0.3 eV over the potential range 0.7−0.9 V. In weak acid Pt and Pt/C electrodes have lower activation energies than the alloys (Table 2) and in strong acid Pt_3Fe/C has generally lower activation energies (Table 3). For the weak acid case, no trends with respect to overpotential seem discernible, but in the strong acid case trends are evident.

IV. Comparison of Theoretical and Experimental Activation Energies: Discusion and Conclusions

All measured activation energies from ref 6 for Pt(111) in 0.05 M sulfuric acid at the reversible potential for the overall four-electron process and from refs 12 and 13 for 0.1 M $HClO_4$ are shown in Figure 1 as open circles. The results of the 1 M TFMSA study are in filled circles and the theoretical curve passes through the filled squares. The theoretical curve used in this work has slightly lower activation energies in the $U > 0.8$ V region than those shown in ref 2, which is a result of additional transition state optimizations.[43] The potentials of the experimental points for perchloric acid have been decreased by using the Nernst equation to correspond to 1 M acid. No attempt has been made to correct for the temperature dependence liquid junction potential in the reference electrode used for the perchloric acid results. As pointed out by Conway and Wilkinson, this can sometimes amount to several tens of millivolts.[44] There was no liquid junction for the reference electrode in the 1 M TFMSA study. The theory curve passes through the column of perchloric acid points at 0.87 V for the alloy electrodes from ref 13 on the theory scale but the points for the carbon supported in perchloric acid particles at lower potentials show no general trend as a group. The errors for these entries are approximately ±2.5 kJ mol^{-1} and may obscure a trend. However, two of the three TFMSA curves show trends similar to the theory curve.

The measured activation energies for 1 M CF_3SO_3H are shown separately in Figure 2 along with the theoretical results. The four points for Pt_3Co/C are closest to paralleling the theory curve and these points have the lowest errors from Arrhenius fits, as may be seen in Table 6. Errors in the data for Pt/C are larger but the trend in activation energies is still similar to the theoretical predictions. Errors are largest for the Pt_3Fe/C case, ranging from 1.5 to 2.9 kJ mol^{-1}, which could be responsible for the lack of trend in these data. Coverage effects may also affect the experimental results. For example, if OH(ads) is the sole adsorbed species and it has coverage $\theta(U)$, then the kinetic current density is given by

$$i_k = A(1 - \theta(U)) \exp[-(E_a(U) + C(U))]/RT \qquad (8)$$

where $E_a(U)$ is the value calculated in the present model, and $C(U)$ is a correction that takes into account variations in reaction center environment with potential. If additional coverage factors due to other adsorbates such as anions and structure factors are included, eq 8 could be modified with additional terms and parameters to model their contributions. For a kinetic modeling study of possible effects of surface coverage by OH(ads) and electrolyte anions on O_2 reduction on platinum, the reader is referred to a recent publication.[45]

Figures 3 and 4 are Tafel plots for the three sputtered polycrystalline electrodes in 0.1 M $HClO_4$ and three supported catalysts in 1 M TFMSA, respectively. It is evident for the polycrystalline electrodes that the plots are similar in form to one another and have well-defined curvature. If there were no coverage preexponential term in eq 8, and if E_a varied linearly in U as in the Bulter−Volmer model, these would be a straight line. Can the curvature in Tafel plots be attributed to the

TABLE 6: Activation Energies for Oxygen Reduction for the Different Electrocatalysts in 1 M CF_3SO_3H as a Function of Electrode Potential

	E_a* (0.70 V)		E_a* (0.75 V)		E_a* (0.80 V)		E_a* (0.85 V)	
catalyst	kJ/mol	eV	kJ/mol	eV	kJ/mol	eV	kJ/mol	eV
Pt/C	19.12 ± 1.80	0.20	22.13 ± 1.70	0.23	26.87 ± 2.00	0.28	27.84 ± 2.04	0.29
PtCo/C	19.02 ± 0.78	0.20	22.33 ± 0.33	0.23	25.18 ± 0.78	0.26	27.86 ± 0.23	0.29
PtFe/C	17.55 ± 2.62	0.18	18.66 ± 1.51	0.19	19.4 ± 2.69	0.20	19.3 ± 2.89	0.20

TABLE 7: Parameters Used in Eq 6 To Obtain the Preexponential Factors *A* to Calculate Activation Energies from the Data of Figures 1 and 2

catalyst	ref	potential (V)	E_a(exp) (eV)	current (mA cm^{-2})	log *A*
in 0.1 M $HClO_4$					
Pt-polycrystalline	13	0.87[a]	0.22	1.656	9.140
Pt_3Co-sputtered	13	0.87[a]	0.23	4.367	10.585
Pt_3Ni-sputtered	13	0.87[a]	0.24	2.760	10.522
in 1 M CF_3SO_3H					
Pt/C	this work	0.85	0.29	0.238	9.992
Pt_3Co/C	this work	0.85	0.29	0.319	10.295
Pt_3Fe/C	this work	0.85	0.20	0.349	6.871

[a] The potentials in this table for 0.1 M $HClO_4$ are 0.06 V less than those in Table 3 in order to align their potential with the 1 M CF_3SO_3H and theory results.

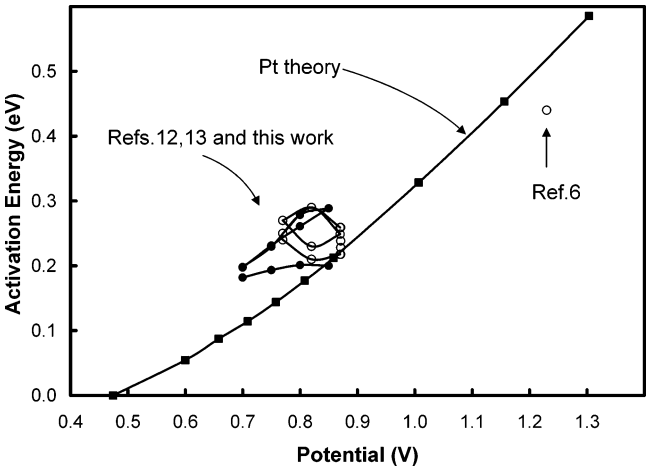

Figure 1. Experimental activation energies (in eV) for O_2 reduction on Pt(111) at the reversible potential from ref 6 (open circle), for carbon-supported Pt, Pt/Ni, and Pt/Co from ref 12 (open circles, see Table 2), for polycrystalline Pt, Pt_3Ni, and Pt_3Co surfaces from ref 13 (open circles, see Table 3), and for carbon-supported Pt, Pt_3Co, and Pt_3Fe (this work, filled circles).

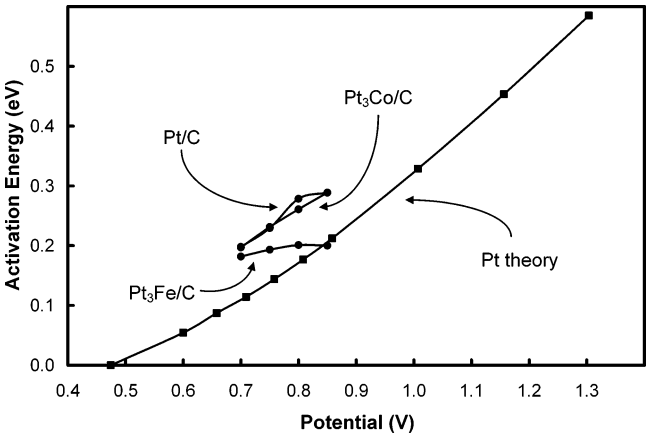

Figure 2. Experimental activation energies (in eV) for carbon-supported Pt, Pt_3Co, and Pt_3Fe in 1 M CF_3SO_3H (this work).

curvature in the potential-dependent activation energies calculated from quantum mechanics in the model of this paper? This would be in the form of a limiting model that excludes explicit coverage parameters. Figure 5 shows the results for the polycrystalline catalysts in perchloric acid where it is seen that over a 150 mV potential range the curvatures of the activation energies derived from Tafel data give curvatures very similar to the curvature of the theoretical plot.

Tafel data for the supported catalysts in 1 M TFMSA in Figure 4 were also converted into activation energies by fitting one of the experimental values, the ones at 0.85 V. The plot in

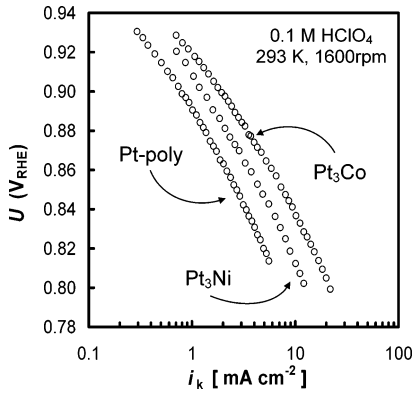

Figure 3. Tafel plots for sputtered surface (without Pt skin): Pt-polycrystalline, Pt_3Co, and Pt_3Ni in 0.1 M $HClO_4$ at 293 K from ref 12.

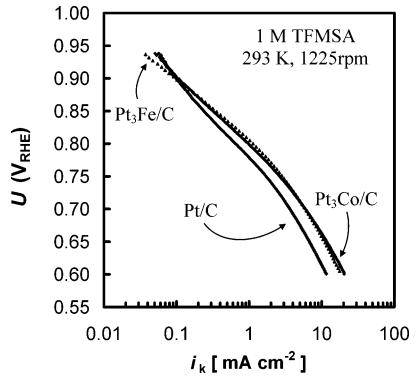

Figure 4. Tafel plots for the ORR at room temperature for Pt-, PtCo-, and PtFe-supported catalysts (this work).

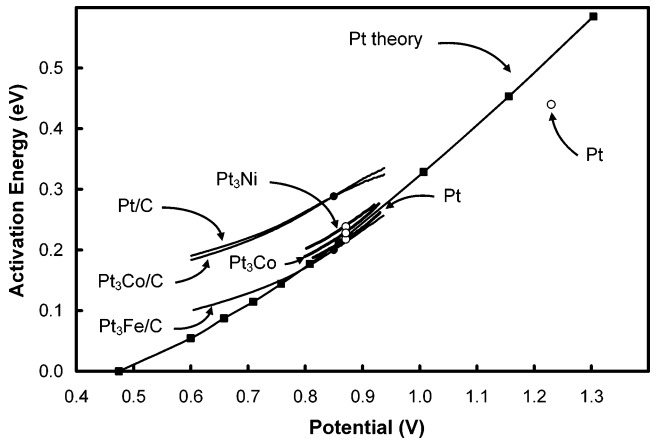

Figure 5. Calculated activation energies from the Tafel plots data in Figures 3 and 4 and from preexponential factor in Table 7. Open circles are for data from ref 13; see Table 3, and the value at the reversible potential is from ref 6. Carbon-supported results from this work pass through filled circles.

Figure 5 shows the resulting curves and the experimental point chosen for each. If the activation energies at 0.7 V had been chosen the curves would be nearly overlapping and all three would be above the theory curve. All of the curvatures are strikingly similar to those for the polycrystalline catalysts in the 0.8−0.9 V range. From 0.8 to 0.6 V the curves seem not to drop toward zero fast enough. This might be due to a too rapid decline for the theoretically calculated activation energies with decreasing potential in this range. All of the curves seem to aim approximately in the direction of the experimental activation energy of 0.44 eV at the reversible potential. This value was based on the temperature dependence of the exchange current

density for a platinum electrode in weak sulfuric acid.[6] These comparisons suggest, assuming the calculated activation energy curve is accurate above 0.8 V, that the number of active sites for all of these catalysts may remain fairly constant as the electrode potential is increased into the OH(ads) formation region. However, the fitting is properly viewed as qualitative and a more complete theory taking all factors into account is needed for distinguishing the relative importance of electrode potential dependent activation energy and coverage effects.

V. Summary

The overall agreement between the perchloric acid and 1 M TFMSA results suggests that (i) the correction for the liquid junction potential in the former is probably small and (ii) for all the different catalysts the active sites for the rate-limiting electroreduction step behave similarly. The overall agreement between the theoretical predictions and the measured current densities suggest that (i) the first electroreduction step, forming OOH(ads), is the rate limiting step and (ii) the active catalyst sites for the various catalyst systems are similar, probably a dual Pt site, and the presence of alloying atoms adjacent to the active site does not dramatically affect the activation energy. The ability to calculate qualitative apparent activation energies as functions of electrode potential from the Tafel plot data suggests that the surface density of active sites may remain fairly constant over the 0.8 to 0.95 V range on all the catalysts.

Acknowledgment. A.B.A. and J.R. acknowledge support for this work by the Department of Energy through a subcontract from U.T.C. Fuel Cells. S.M. and V.S.M. gratefully acknowledge the financial support from the Army Research Office (Single Investigator and a Multi-University Research Initiative Grant). S.M. also gratefully acknowledges support from the Department of Energy, Materials Science Division for building and maintaining the National Synchrotron Light Source at Brookhaven National Laboratory, Upton, NY (beam line X-11A). N.M.M. and V.R.S. acknowledge the support by the Director, Office of Science, Division of Materials Sciences, U.S. Department of Energy under Contract No. DE-AC03-76SF00098.

References and Notes

(1) Albu, T. V.; Anderson, A. B. *J. Electrochem. Soc.* **2000**, *147*, 4229.
(2) Sidik, R. A.; Anderson, A. B. *J. Electroanal. Chem.* **2002**, *528*, 69.
(3) Anderson, A. B.; Kang, D. B. *J. Phys. Chem. A* **1998**, *102*, 5993.
(4) Anderson, A. B.; Albu, T. V. *Electrochem. Commun.* **1999**, *1*, 203.
(5) Anderson, A. B.; Albu, T. V. *J. Am. Chem. Soc.* **1999**, *121*, 11855.
(6) Grgur, B. N.; Markovic, N. M.; Ross, P. N. *Can. J. Chem*. **1997**, *74*, 1465.
(7) Iwasita, T.; Xia, X. *J. Electroanal. Chem.* **1996**, *411*, 95.
(8) Markovic, N. M.; Schmidt, T. J.; Grgur, B. N.; Gasteiger, H. A.; Behm, R. J.; Ross, P. N. *J. Phys. Chem. B* **1999**, *103*, 8568.
(9) Markovic, N. M.; Ross, P. N. in *Interfacial Electrochemistry. Theory, Experiment and Applications*; Wieckowski, Ed.; Marcel Dekker: New York, 1999; p 821.
(10) Mukerjee, S.; Srinivasan, S.; Soriaga, M. P.; McBreen, J. *J. Electrochem. Soc.* **1995**, *142*, 1409.
(11) Mukerjee, S.; Srinivasan, S. *J. Electroanal. Chem.* **1993**, *357*, 201.
(12) Paulus, U. A.; Wokaun, A.; Scherer, G. G.; Schmidt, T. J.; Stamenkovic, V.; Radmilovic, V.; Markovic, N. M.; Ross, P. N. *J. Phys. Chem. B* **2002**, *106*, 4181.
(13) Stamenkovic, V.; Schmidt, T. J.; Ross, P. N.; Markovic, N. M. *J. Phys. Chem. B* **2002**, *106*, 11970.
(14) Murthi, V. S.; Urian, R. C.; Mukerjee, S. *J. Phys. Chem. B* **2004**, *108*, 537.
(15) Frisch, M. J.; Trucks, G. W.; Schlegel, H. B.; Gill, P. M. W.; Johnson, B. G.; Robb, M. A.; Cheeseman, J. R.; Keith, T.; Petersson, G. A.; Montgomery, J. A.; Raghavachari, K.; Al-Laham, M. A.; Zakrzewski, V. G.; Ortiz, J. V.; Foresman, J. B.; Cioslowski, J.; Stefanov, B. B.; Nanayakkara, A.; Challacombe, M.; Peng, C. Y.; Ayala, P. Y.; Chen, W.; Wong, M. W.; Andres, J. L.; Replogle, E. S.; Gomperts, R.; Martin, R. L.; Fox, D. J.; Binkley, J. S.; Defrees, D. J.; Baker, J.; Stewart, J. P.; Head-Gordon, M.; Gonzalez, C.; Pople, J. A. *Gaussian 94*, Revision C.3; Gaussian Inc.: Pittsburgh, PA, 1995.
(16) Bockris, J. O.; Khan, S. U. M. *Surface Electrochemistry*: *Molecular Level Approach*; Plenum: New York, 1993; p 319.
(17) Kostadinov, L. N.; Anderson, A. B. *Electrochem. Solid-State Lett.* **2003**, *6*, E30.
(18) Kang, D. B.; Cai, Y.; Anderson, A. B. Unpublised results.
(19) Jalan, V. M.; Bushnell, C. L. United Technologies Corp., USA; U.S., Us 1979; p 4.
(20) Jalan, V. M. Giner, Inc., USA, Eur. Pat. Appl. Ep 1985; p 10.
(21) Landsman, D. A.; Luczak, F. J. United Technologies Corp., USA; Belg., Be, 1981; p 16.
(22) Stonehart, P.; Watanabe, M.; Yamamoto, N.; Nakamura, T.; Hara, N.; Tsurumi, K. Stonehart Associates Inc., USA; Jpn. Kokai Tokkyo Koho, Jp 1992; p 5.
(23) Mukerjee, S. *J. Appl. Electrochem.* **1990**, *20*, 537.
(24) Gong, S.; Lu, J.; Yan, H. *J. Electroanal. Chem.* **1997**, *436*, 291.
(25) Will, F. G. *J. Electrochem. Soc.* **1986**, *133*, 454.
(26) Lee, H. S.; Yang, X. O.; McBreen, J.; Xiang, C. Brookhaven Science Associates, USA; U.S., Us 2000; p 11.
(27) Paulus, U. S.; Schmidt, T. J.; Gasteiger, H. A.; Behm, R. J. *J. Electroanal. Chem.* **2001**, *495*, 134.
(28) Gojkovic, S. L.; Zecevic, S. K.; Savinell, R. F. *J. Electrochem. Soc.* **1998**, *145*, 3713.
(29) Zecevic, S. K.; Wainright, J. S.; Litt, M. H.; Gojkovic, S. L.; Savinell, R. F. *J. Electrochem. Soc.* **1997**, *144*, 2973.
(30) Wong, J.; Lytle, F. W.; Messmer, R. P.; Maylotte, D. H. *Phys. Rev. B*: *Condens. Matter Mater. Phys.* **1984**, *30*, 5596.
(31) McBreen, J. *Phys. Electrochem.* **1995**, 339.
(32) McBreen, J.; Mukerjee, S. *J. Electrochem. Soc.* **1995**, *142*, 3399.
(33) Zon, J. B. A. D. V.; Koningsberger, D. C.; Van't Blik, H. F. J.; Sayers, D. E. *J. Chem. Phys.* **1985**, *82*, 5742.
(34) Duivenvoorden, F. B. M.; Koningsberger, D. C.; Uh, Y. S.; Gates, B. C. *J. Am. Chem. Soc.* **1986**, *108*, 6254.
(35) Mukerjee, S.; Urian, R. C. *Electrochim. Acta* **2002**, *47*, 3219.
(36) Mukerjee, S.; Srinivasan, S.; Soriaga, M. P.; McBreen, J. *J. Phys. Chem.* **1995**, *99*, 4577.
(37) Markovic, N. M.; Gasteiger, H. A.; Ross, P. N. *J. Phys. Chem.* **1995**, *99*, 3411.
(38) Uribe, F. A.; Springer, T. E.; Gottesfeld, S. *J. Electrochem. Soc.* **1992**, *139*, 765.
(39) Gonzalez, E. R.; Srinivasaan, S. *Electrochim. Acta* **1982**, *27*, 1425.
(40) Ross, P. N.; Andricacos, P. C. *J. Electroanal. Chem. Interfacial Electrochem.* **1983**, *154*, 205.
(41) Kotz, R.; Clouser, S.; Sarangapani, S.; Yeager, E. *J. Electrochem. Soc.* **1984**, *131*, 1097.
(42) Zelenay, P.; Habib, M. A.; Bockris, J. O. M. *J. Electrochem. Soc.* **1984**, *131*, 2464.
(43) Sidik, R. A. Unpublished results.
(44) Conway, B. E.; Wilkinson, D. P. *Electrochim. Acta* **1993**, *38*, 997.
(45) Wang, J. X.; Markovic, N. M.; Adzic, R. R. *J. Phys. Chem. B* **2004**, *108*, 4127.